VIRTUAL SOURCE PATTERNS FOR FLUORESCENCE TOMOGRAPHY

N. Ducros[1]*, A. Bassi*[1]*, C. D'Andrea*[1,2]*, G. Valentini*[1] *M. Schweiger*[3]*, and S. Arridge*[3]

[1] Instituto di Fotonica e Nanotecnologie (IFN-CNR);
Dipartimento di Fisica, Politecnico di Milano, Piazza Leonardo da Vinci 32, I-20133 Milan, Italy.
[2] Italian Institute of Technology (IIT), Piazza Leonardo da Vinci 32, I-20133 Milan, Italy.
[3] Centre for Medical Image Computing, University College London,
Malet Place, London WC1E 6BT, United Kingdom.

ABSTRACT

In order to reduce both acquisition and reconstruction times, illumination and detection in fluorescence molecular tomography have recently evolved from a point-based to a pattern-based approach. However, the choice of the best set of source patterns to project onto the sample is still an open problem. Here, we introduce a novel method, namely the virtual source patterns method, which allows for considering patterns with negative intensities. This method is shown to significantly increase the contrast and to reduce the reconstruction error.

***Index Terms*—** Fluorescence molecular tomography, structured light, source pattern choice, reconstruction.

1. INTRODUCTION

In the last years, the rapid development of specifically designed optical markers and technological improvements of imaging system, has fostered the field of optical molecular imaging [1]. The main challenge of this modality is to deal with thick tissues for which the images appear blurred due to scattering. Moreover, projective imaging inherently suffers from a lack of depth resolution. Fluorescence molecular tomography (FMT) has been designed to solve this couple of problems by allowing to reconstruct the three-dimensional (3-D) fluorescence distribution within the sample ([2, 3, 4, 5]).

In the last years, different research groups have begun to study the possibility to increase the speed of FDOT reducing the data-set without sacrificing the reconstruction quality [6, 7, 8]. First, a series of works have capitalized on the low-pass filtering of the spatial frequencies of light propagating in highly scattering medium [6, 9]. Fluorescent images obtained from biological tissue can be compressed to few coefficients with little degradation considering adapted bases like Fourier [10, 11] or wavelets [12, 13, 14]. Second, it has been proposed to adopt patterns of illumination instead of point sources [6, 15, 16, 17, 8, 18]. Indeed, few well-chosen patterns can be used to acquire as much information as a dense raster scanning of a point source [17, 13]. In this context, we have proposed a fast reconstruction algorithm able to deal with arbitrary geometries. It has been demonstrated with experimental data acquired from a slab [13] and from a cylinder [14]. Recently, a similar approach was used applied in the time domain to the mouse [19].

An open problem lies in the choice of the most appropriate set of source patterns to be projected onto the sample. Up to now many types of source patterns have been proposed. Among them, uniform patterns [16], *ad hoc* patterns (moving bars [16, 20], scanning Gaussians and diffractive optics patterns [15], checkerboard [20]), Sinusoidal patterns [6, 7, 8, 10, 11], and wavelets patterns [13, 14]. A fundamental step has been made by [18] who provided optimal source patterns for a slab, a cylinder, and a numerical phantom simulating the optical properties of animal models (Digimouse). Nonetheless, it remains unclear how the choice of the source pattern translates in terms of reconstruction quality, especially when experimental data are considered.

In this paper, we compare the typically-used source patterns. In particular, it will be shown that even if different source patterns are used the reconstruction quality is similar to that obtained with with a uniform illumination. To fully take advantage of the structured illumination, a method able to exploit the tissue response to any negative pattern is introduced. In Section 2, we first formulate the forward problem of FMT. Then, the method enabling to consider arbitrary patterns is presented. It is referred to as virtual source pattern (VSP) method. Last, the main steps of our reconstruction algorithm are described. In Section 4, we present three experiments. The first two cases deal with actual sources patterns and the last one implements virtual source patterns. The reconstruction results are discussed in Section 5 and our conclusions are reported in Section 6.

2. METHOD

2.1. Forward Problem

We consider a medium Ω embedding a fluorescence distribution $f(\mathbf{r})$ to be recovered. A portion $\partial\Omega^x$ of the medium surface is illuminated with a source pattern pattern $\mathbf{s}$. The fluorescence light exiting through the surface $\partial\Omega^f$ is recorded by a CCD camera and the image $\mathbf{m}$ is obtained. To reduce the dimensionality of the problem, the fluorescence image $\mathbf{m}$ is transformed to $\hat{\mathbf{m}} = \sum_k \hat{m}_k \mathbf{d}_k$ and only the K largest components $\hat{m}_k$ are retained. Provided an appropriate transform (e.g. wavelet), this results in little degradation. The images $\mathbf{d}_k$ are referred to as detection patterns.

The forward problem in FDOT consists in determining the image component $\hat{m}_k$ for any fluorescence distribution $f(\mathbf{r})$, given the source pattern $\mathbf{s}$ and detection pattern $\mathbf{d}_k$. In a general problem, the object is rotated and different patterns are used for each view. We note I the number of rotation angles and J the number of source patterns considered for each angle. Therefore, a set IJ images is acquired and IJK image components are retained. The forward problem in FDOT is inherently linear. Discretizing the volume Ω into N voxels, we have the following linear problem:

$$\hat{\mathbf{m}} = \mathbf{W}\mathbf{f}. \tag{1}$$

In the latter, $\hat{\mathbf{m}} \in \mathbb{R}^{IJK}$ is the measurement vector containing the

retained image components, $\mathbf{f} \in \mathbb{R}^N$ is the discrete fluorescence distribution, and $\mathbf{W} \in \mathbb{R}^{IJK \times N}$ is the weight matrix. The calculation of the weight matrix mainly requires an appropriate model for light propagation, e.g., the diffusion approximation.

2.2. Virtual source patterns method

Only patterns with positive intensities can be projected on the sample. Despite this constrain, we describe a simple method that offers the possibility to exploit the response to any pattern (negative or complex). The so-called virtual source patterns (VSP) method exploits the linearity of the forward problem. Indeed, the fluorescence image $\mathbf{m}$ resulting from source $\mathbf{s} = \mathbf{s}_1 + \mathbf{s}_2$ may be obtained as the sum $\mathbf{m} = \mathbf{m}_1 + \mathbf{m}_2$, where $\mathbf{m}_1$ and $\mathbf{m}_2$ are the images resulting from the source patterns $\mathbf{s}_1$ and $\mathbf{s}_2$, respectively.

Let $\tilde{\mathbf{S}} = [\tilde{\mathbf{s}}_1 \dots \tilde{\mathbf{s}}_{\tilde{J}}]$ represent the $\tilde{J}$ (desired) virtual source patterns. Our approach consist in finding J actual source patterns $\mathbf{S} = [\mathbf{s}_1 \dots \mathbf{s}_J]$ and a $\tilde{J} \times J$ (possibly complex) matrix $\mathbf{T}$ such that

$$\tilde{\mathbf{S}}^T = \mathbf{T}\mathbf{S}^T. \tag{2}$$

The matrix $\mathbf{T}$ is referred to as transformation matrix. By the sake of linearity, the same transformation can be applied to the actual measurements $\mathbf{M} = [\mathbf{m}_1 \dots \mathbf{m}_J]$ so as to get the virtual measurements $\tilde{\mathbf{M}} = [\tilde{\mathbf{m}}_1 \dots \tilde{\mathbf{m}}_{\tilde{J}}]$ that would have been measured if the virtual patterns $\tilde{\mathbf{S}}$ were projected onto the medium. Formally:

$$\tilde{\mathbf{M}}^T = \mathbf{T}\mathbf{M}^T. \tag{3}$$

2.3. Reconstruction algorithm

2.3.1. Preprocessing

For every view i, the $\tilde{J}$ virtual source patterns $\tilde{\mathbf{s}}_{i,\tilde{\jmath}}$ and the $\tilde{J}$ virtual fluorescence images $\tilde{\mathbf{m}}_{i,\tilde{\jmath}}$ are calculated according to (2) and to (3), respectively. Then, any of the $I\tilde{J}$ virtual fluorescence image $\tilde{\mathbf{m}}_{i,\tilde{\jmath}}$ is wavelet transformed to $\hat{\mathbf{m}}_{i,\tilde{\jmath}} = \sum_k \hat{m}_{i,\tilde{\jmath},k}\mathbf{d}_{i,\tilde{\jmath},k}$ and the K (absolute value) largest components $\hat{m}_{i,\tilde{\jmath},k}$ are retained. A set of $I\tilde{J}K$ detection pattern $\mathbf{d}_{i,\tilde{\jmath},k}$ is obtained.

2.3.2. Construction of the weight matrix

The weight matrix $\mathbf{W} \in \mathbb{R}^{IJK \times N}$ is computed row by row. The vector $\mathbf{w}_{i,\tilde{\jmath},k}$ denotes the row of the weight matrix $\mathbf{W}$ corresponding to the triplet $(i, \tilde{\jmath}, k)$, i.e., $\mathbf{w}_{i,\tilde{\jmath},k}$ satisfies $\hat{m}_{i,\tilde{\jmath},k} = \mathbf{w}_{i,\tilde{\jmath},k}^T\mathbf{f}$. It is obtained by

$$\mathbf{w}_{i,\tilde{\jmath},k} = \boldsymbol{\varphi}_{i,\tilde{\jmath}} \circ \boldsymbol{\psi}^*_{i,\tilde{\jmath},k}, \tag{4}$$

where $\circ$ stands for the entrywise (Hadamard) product. The vector $\boldsymbol{\varphi}_{i,\tilde{\jmath}} \in \mathbb{R}^N$ must be calculated for all couples $(i, \tilde{\jmath})$ and the vector $\boldsymbol{\psi}_{i,\tilde{\jmath},k} \in \mathbb{R}^N$ for any triplet $(i, \tilde{\jmath}, k)$. These two vectors respectively solve

$$\mathbf{P}\boldsymbol{\varphi}_{i,\tilde{\jmath}} = \tilde{\mathbf{s}}_{i,\tilde{\jmath}} \quad \text{and} \quad \mathbf{P}\boldsymbol{\psi}_{i,\tilde{\jmath},k} = \mathbf{d}_{i,\tilde{\jmath},k}. \tag{5}$$

where $\mathbf{P} \in \mathbb{R}^{N \times N}$ is a sparse matrix that models light propagation. Here, $\mathbf{P}$ is obtained thanks to the Matlab TOAST package [21].

2.3.3. Resolution of inverse problem

The inverse problem in FDOT is well-known to be ill-posed and requires regularization to ensure the stability of the solution $f^\star$ in the presence of noise. Here, the inverse problem is efficiently solved considering the *underdetermined* Tikhonov solution

$$\mathbf{f}^\star = \mathbf{W}^T(\mathbf{W}\mathbf{W}^T + \alpha\mathbf{I})^{-1}\hat{\mathbf{m}} \tag{6}$$

where α is the regularization parameter that enforces the stability of the solution.

2.4. Figures of merit

Two figures of merit are considered: the contrast-to-noise ratio (CNR) and the reconstruction error. The CNR, which indicates how well structures of interest are rendered in a reconstruction, is defined by

$$CNR = \frac{\mu_{roi} - \mu_{back}}{(w_{roi}\sigma^2_{roi} + w_{back}\sigma^2_{back})^{1/2}}, \tag{7}$$

where μ_{roi} (μ_{back}) and σ_{roi} (σ_{back}) are the average and standard deviation of $\mathbf{f}^\star$ in the region of interest (background). The weights w_{roi} and w_{back} are the volume ratios $w_{roi} = V_{roi}/V_{tot}$ and $w_{back} = V_{back}/V_{tot}$. Here, the region of interest refers to the volume occupied by the fluorescence inclusions and the background refers to the rest of the volume.
The reconstruction error $\mathcal{E}_r$, expressed in decibels, is defined by

$$\mathcal{E}_r(\text{dB}) = 20\log\|\mathbf{f}^\star\frac{\mu_{roi}}{\mu^\star_{roi}} - \mathbf{f}_{ref}\| - 20\log\|\mathbf{f}_{ref}\|. \tag{8}$$

3. SAMPLE AND EXPERIMENTAL SET-UP

Our phantom is an epoxy resin cylinder of radius 20 mm and height 45 mm. At $\lambda^x = 630$ nm, the following absorption coefficient and reduced scattering coefficient have been measured: $\mu_a = 0.022$ mm^{-1} $\mu'_s = 1.35$ mm^{-1}. The phantom holder is mounted on a motorized rotational stage in order to perform multiple view measurements.

The experimental set-up, which has been described in details in [10], is based on two main components: illumination device, and detection system. Light is emitted by a He:Ne laser source (05LHP991, Melles Griot) at 633 nm, coupled to an optical fiber guide (LLG0538-4, Thorlabs), and delivered to a Digital Micromirror Device (DMD) (Discovery 1100 - ALP1, Vialux). By uploading the image of the desired spatial pattern, the light beam reflected by the DMD change accordingly. The pattern is magnified and projected onto the phantom within a rectangular illumination area $\partial\Omega^x$ of width $\ell_x = 13$ mm and height $\ell_y = 26$ mm.

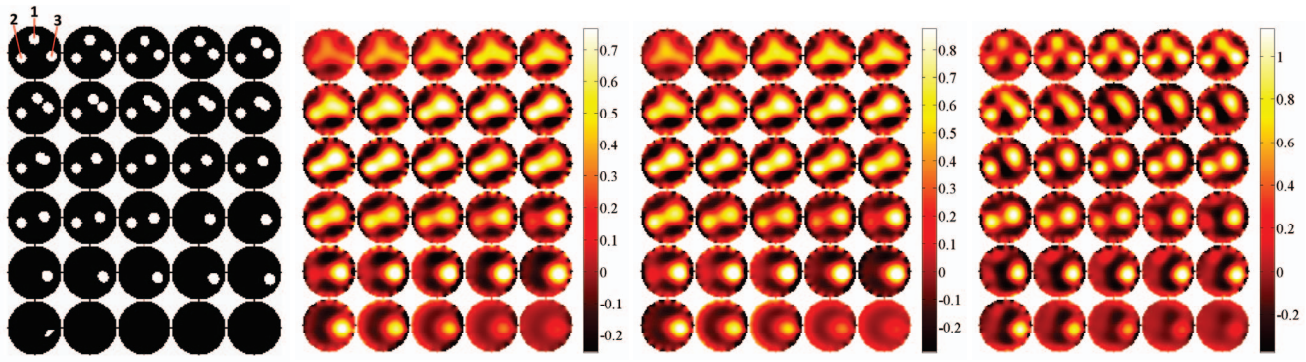
The light exiting the opposite side of the phantom is imaged by an objective lens ($f = 50$ mm, $f\#= 2.8$, Nikon Co.) on a low noise high sensitivity 16 bit CCD camera (Versarray 512, Princeton Instruments,) cooled to $-40\,^\circ$C. An interference filter (XF 3076, Omega) together with a high pass filter (RG-695, Schott) is placed in front of the objective lens.

4. RESULTS

We present three experiments. The first two experiments implement real source patterns while the last implement virtual source patterns. Experiments have been performed in the same conditions, i.e., every source pattern has been projected for 35 s and $I = 16$ rotation angles from $0\,^\circ$ to $337.5\,^\circ$ have been considered. The performance metrics for each experiment are reported in table 1.

4.1. Case 1 – Uniform illumination

The fist experiment is performed loading onto the DMD a constant image whose intensity level is set to the maximum value (255). This experiment is a reference experiment, which enables for measuring the highest signal in transmission. Indeed, the zero spatial frequency



(a) (b) (c) (d)

Fig. 2. Phantom and reconstructions. Slices are displayed every millimeter from $z = 19.5$ mm (top left) to $z = -9.5$ mm (bottom right). a) phantom; b) reconstruction of case 1: uniform source pattern; c) reconstruction of case 2: eight scaling functions; d) reconstruction of case 3: six wavelet functions.

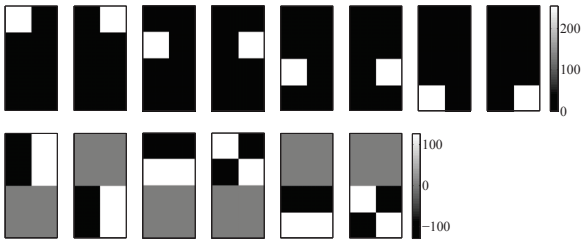


Fig. 1. Source patterns. Top row: case 2; bottom row: case 3.

Table 1. Performance metrics for the different illumination patterns

Case	CNR	$\mathcal{E}_r$ (dB)
1	2.10	-17.2
2	2.13	-18.1
3	2.76	-19.0

is the less attenuated one (see for example [9]). The whole set of reconstruction slices is depicted in figure 2.

4.2. Case 2 – Haar scaling functions

In this experiment, we consider 2-D scaling functions of wavelets. It is well known that such 2-D functions can provide a multiresolution approximation of images. Among wavelet bases, B-spline wavelets interestingly provide positive scaling functions that can be actually loaded onto the DMD. In this experiment, we consider the Haar wavelet that is noting but zeroth-order B-spline wavelet. At scale 2, the patterns simplify to black images containing a white square of side $\ell_y/2 = \ell_y/4$. The source patterns are displayed in the top row of figure 1. The reconstructed fluorescence distribution obtained from eight Haar scaling patterns is presented at figure 2c.

4.3. Case 3 – Virtual Haar wavelets

While scaling functions are used in case 3, wavelet functions are desired in this experiment. Wavelet functions possess a higher frequency content than scaling functions and provide details (at different scale) in image compression. Implementing such patterns requires the VSP method since wavelets contain negative values. Interestingly, wavelet functions at a given scale are easily obtained from scaling functions at a lower scale. Capitalizing on this property, the measurements of case 3 can serve in this experiment to get the response to scale 1 Haar wavelet patterns. The transformation matrix to be used is given by:

$$\mathbf{T} = \begin{pmatrix} -1 & 1 & -1 & 1 & 0 & 0 & 0 & 0 \\ 0 & 0 & 0 & 0 & -1 & 1 & -1 & 1 \\ -1 & -1 & 1 & 1 & 0 & 0 & 0 & 0 \\ 1 & -1 & -1 & 1 & 0 & 0 & 0 & 0 \\ 0 & 0 & 0 & 0 & -1 & -1 & 1 & 1 \\ 0 & 0 & 0 & 0 & 1 & -1 & -1 & 1 \end{pmatrix}. \quad (9)$$

The virtual source patterns, i.e., the columns of $\tilde{\mathbf{S}} = \mathbf{TS}$ are displayed in the bottom row of figure 1. The reconstruction of the fluorescence distribution from the virtual Haar wavelets is available in figure 2c.

5. DISCUSSION

Using only a uniform illumination, the overall quality of the reconstruction is quite good. Inclusion 2 is reconstructed with a correct localization in the xy plan as well as along z. However, the reconstruction of inclusions 1 and 3 is of lower quality, especially in top slices down to $z = 9.5$ mm, where inclusion 1 joins inclusion 3. Reconstructed fluorescence is observed to vanish in the first top slices (from $z = 19.5$ mm to $z = 17.5$ mm, in particular). The latter effect is a typical problem that can be attributed to the vicinity of boundary. By visual inspection of the reconstruction slices displayed in figure 2c, the benefit of using 8 source patterns appears limited. The figures of merit reported in table 1 exhibits a slight improvement with a diminution of the reconstruction error and an augmentation of the CNR. Comparing the first two cases to the third one (compare figure 2b and figure 2c to figure 2d), it can be seen that the VSP method outperforms the direct method. In particular,

inclusion 1 is nicely individuated and the first three slices show little blurring. These visual observations are confirmed by the figures of merits reported in table 1.

A key feature of the VSP method lies in its ability to remove the DC components in the fluorescence images. Indeed, in experimental scenarios removing the DC component is highly profitable since it permits to cancel out undesirable light. To capitalize on this feature, a satisfying transformation matrix must low-pass filter the actual fluorescence images. Hence, the sum of coefficients of every row of the transformation matrix $\mathbf{T}$ must equal zero. The transformation matrix of case 3 (see (9)) has been chosen to satisfy this condition.

6. CONCLUSIONS

This work addresses the problem of the choice of the source patterns in fluorescence molecular tomography considering experimental measurements. We have shown that using different source patterns limited to positive values provide very similar reconstructions. The so-called virtual source pattern (VSP) method, which allows for considering any source pattern, alleviates this problem. Virtual patterns corresponding to Haar wavelet functions are shown to improve significantly the reconstruction. It is worth outlying that the VSP method has also the ability to reject undesirable light. In future work, we will investigate the benefit of the proposed method in small animal imaging.

7. REFERENCES

[1] Simon R Cherry, "In vivo molecular and genomic imaging: new challenges for imaging physics," *Physics in Medicine and Biology*, vol. 49, no. 3, pp. R13, 2004.

[2] V. Ntziachristos, J. Ripoll, L.V. Wang, and R. Weissleder, "Looking and listening to light: the evolution of whole-body photonic imaging," *Nature Biotechnology*, vol. 23, no. 3, pp. 313–320, 2005.

[3] Anne Koenig, Lionel Herve, Veronique Josserand, Michel Berger, Jerome Boutet, Anabela Da Silva, Jean-Marc Dinten, Philippe Peltie, Jean-Luc Coll, and Philippe Rizo, "In vivo mice lung tumor follow-up with fluorescence diffuse optical tomography," *Journal of Biomedical Optics*, vol. 13, no. 1, pp. 011008, 2008.

[4] A. T. N. Kumar, S. B. Raymond, A. K. Dunn, B. J. Bacskai, and D. A. Boas, "A time domain fluorescence tomography system for small animal imaging," *Medical Imaging, IEEE Transactions on*, vol. 27, no. 8, pp. 1152–1163, Aug. 2008.

[5] Alexander D Klose and Thomas Pschinger, "Excitation-resolved fluorescence tomography with simplified spherical harmonics equations," *Physics in Medicine and Biology*, vol. 56, no. 5, pp. 1443, 2011.

[6] David J. Cuccia, Frederic Bevilacqua, Anthony J. Durkin, and Bruce J. Tromberg, "Modulated imaging: quantitative analysis and tomography of turbid media in the spatial-frequency domain," *Opt. Lett.*, vol. 30, no. 11, pp. 1354–1356, 2005.

[7] Andrea Bassi, Cosimo D'Andrea, Gianluca Valentini, Rinaldo Cubeddu, and Simon Arridge, "Detection of inhomogeneities in diffusive media using spatially modulated light," *Opt. Lett.*, vol. 34, no. 14, pp. 2156–2158, 2009.

[8] Soren D. Konecky, Amaan Mazhar, David Cuccia, Anthony J. Durkin, John C. Schotland, and Bruce J. Tromberg, "Quantitative optical tomography of sub-surface heterogeneities using spatially modulated structured light," *Opt. Express*, vol. 17, no. 17, pp. 14780–14790, 2009.

[9] Andrea Bassi, Cosimo D'Andrea, Gianluca Valentini, Rinaldo Cubeddu, and Simon Arridge, "Temporal propagation of spatial information in turbid media," *Opt. Lett.*, vol. 33, no. 23, pp. 2836–2838, 2008.

[10] Cosimo D'Andrea, Nicolas Ducros, Andrea Bassi, Simon Arridge, and Gianluca Valentini, "Fast 3d optical reconstruction in turbid media using spatially modulated light," *Biomed. Opt. Express*, vol. 1, no. 2, pp. 471–481, 2010.

[11] Jorge Ripoll, "Hybrid fourier-real space method for diffuse optical tomography," *Opt. Lett.*, vol. 35, no. 5, pp. 688–690, 2010.

[12] Timothy J. Rudge, Vadim Y. Soloviev, and Simon R. Arridge, "Fast image reconstruction in fluoresence optical tomography using data compression," *Opt. Lett.*, vol. 35, no. 5, pp. 763–765, 2010.

[13] Nicolas Ducros, Cosimo D'andrea, Gianluca Valentini, Tim Rudge, Simon Arridge, and Andrea Bassi, "Full-wavelet approach for fluorescence diffuse optical tomography with structured illumination," *Opt. Lett.*, vol. 35, no. 21, pp. 3676–3678, 2010.

[14] Nicolas Ducros, Andrea Bassi, Gianluca Valentini, Martin Schweiger, Simon Arridge, and Cosimo D'Andrea, "Multiple-view fluorescence optical tomography reconstruction using compression of experimental data," *Opt. Lett.*, vol. 36, no. 8, pp. 1377–1379, Apr 2011.

[15] Amit Joshi, Wolfgang Bangerth, Kildong Hwang, John Rasmussen, and Eva M. Sevick-Muraca, "Plane-wave fluorescence tomography with adaptive finite elements," *Opt. Lett.*, vol. 31, no. 2, pp. 193–195, Jan 2006.

[16] Amit Joshi, Wolfgang Bangerth, and Eva M. Sevick-Muraca, "Non-contact fluorescence optical tomography with scanning patterned illumination," *Opt. Express*, vol. 14, no. 14, pp. 6516–6534, 2006.

[17] Vladimir Lukic, Vadim A. Markel, and John C. Schotland, "Optical tomography with structured illumination," *Opt. Lett.*, vol. 34, no. 7, pp. 983–985, 2009.

[18] Joyita Dutta, Sangtae Ahn, Anand A Joshi, and Richard M Leahy, "Illumination pattern optimization for fluorescence tomography: theory and simulation studies," *Physics in Medicine and Biology*, vol. 55, no. 10, pp. 2961, 2010.

[19] Jin Chen, Vivek Venugopal, Frederic Lesage, and Xavier Intes, "Time-resolved diffuse optical tomography with patterned-light illumination and detection," *Opt. Lett.*, vol. 35, no. 13, pp. 2121–2123, Jul 2010.

[20] S. Bélanger, M. Abran, X. Intes, C. Casanova, and F. Lesage, "Real-time diffuse optical tomography based on structured illumination," *Journal of Biomedical Optics*, vol. 15, no. 1, pp. 016006, 2010.

[21] M. Schweiger and S. R. Arridge, ," *TOAST package,* `http://web4.cs.ucl.ac.uk/research/vis/toast/`, 2010.